Morphological instabilities of a nonequilibrium nematic-isotropic interface

J. M. A. Figueiredo and O. N. Mesquita*

Departamento de Física, Instituto de Ciências Exatas, Universidade Federal de Minas Gerais, Caixa Postal 702, Belo Horizonte, 30161-960, Minas Gerais, Brazil

(Received 18 August 1995; revised manuscript received 30 October 1995)

We present a detailed account of our videomicroscopy experiments on morphological instabilities of the nonequilibrium nematic-isotropic interface of the liquid crystal 8CB. For the parameter region chosen in our experiments, the time evolution of the amplitude of the most unstable spatial mode of the interface, during the planar-cellular bifurcation, can be well described by a third-order Landau-amplitude equation. Instability growth rates and cubic coefficients are in agreement with the two-sided model of solidification. Interface kinetics was also considered. In addition, we have made an analytical calculation of the Eckhaus boundary for solidification models. Even though we use an amplitude equation in our calculation, we have obtained a tilted Eckhaus boundary. This feature was previously believed to show up only in numerical calculations of complete models of solidification. We attempt to explain the final wave vectors measured in our experiments based on an Eckhaus instability. Another selection mechanism is mentioned.

PACS number(s): 61.30.Jf, 81.30.Fb, 05.70.Ln

I. INTRODUCTION

The search for universal behavior in nonequilibrium systems, and the necessity of a more general theoretical framework to deal with the wide range of phenomena observed, has demanded controlled experiments carried out systematically in different prototype systems. Traditionally, hydrodynamic systems have received most of the attention. The amount of data about Rayleigh-Bénard or Taylor-Couette instabilities is large and has contributed enormously to the present understanding of pattern formation outside of equilibrium, transition to chaos, and turbulence. In order to check the universal character of some of the phenomena observed and the theoretical predictions, one has to study other prototype systems.

Recently, Cross and Hohenberg published a review on pattern formation outside of equilibrium, with a thorough discussion about the many systems studied up to now and with an updated view of the theoretical methods used in this field of research [1].

Solidification of thin samples of pure or binary mixtures has become an important prototype system to study pattern formation outside of equilibrium and instabilities with complex dynamics. In this case, the motion and shape of the interface between two different thermodynamic phases is the subject of study. It is at the interface that a first-order phase transition takes place,and consequently, where the important physical processes occur. If the interface is moving towards a metastable phase, instabilities can occur and the interface, initially planar, may turn into one with a more complex shape.

*Author to whom correspondence should be addressed. Electronic address: omeskita@oraculo.lcc.ufmg.br

A linear stability analysis of the planar-cellular bifurcation, during solidification of pure and alloy systems, was first performed by Mullins and Sekerka (MS) [2]. The linear analysis is important to identify the physical mechanism of the instability, to determine the important length scales of the problem, and the values of the critical parameters. In the case of directional solidification of binary mixtures, the sample is pulled with constant velocity under a constant temperature gradient, as shown in Fig. 1. The important control parameters, which can be externally adjusted, are the pulling velocity, the temperature gradient, and the solute concentration of the mixture. The available theories consider solidification in two-dimensional systems. Experimental realization of this geometry is accomplished with the use of very thin samples (of the order of a few μm), sandwiched between microscope glass slides. Clearly, this is an approximation and the third dimension (thickness of the sample) may have some influence on the results. Comparison between the results of the linear analysis and experimental data is reliable near the onset of the instability. The linear analysis is unable to predict the final shape of the interface.

A weakly nonlinear stability analysis of the planar-cellular bifurcation of alloys during directional solidification was performed by Wollkind and Segel (WS) [3], in order to determine the nature of the bifurcation. The one-sided model of solidification, where diffusion of impurities in the solid is neglected, was considered. Their main conclusion was that, for usual alloys, the planar-cellular bifurcation is subcritical: the interface is linearly stable and the instability occurs for finite deformation amplitudes of the interface. This is to be compared to the case of a supercritical bifurcation where the instability initiates with infinitesimal deformation amplitudes of the interface. As a consequence, the amplitude of the cellular pattern originated from a subcritical bifurcation is al-

ready large, well within the nonlinear regime, where the Mullins-Sekerka predictions are no longer valid.

Much effort has been devoted to check the Mullins-Sekerka predictions for various alloy systems. Cheveigné *et al.* [4] compiled much of the existing data for alloy solidification and were able to identify two classes of systems: one with cellular structures whose wavelength, at the onset of the instability, satisfies the Mullins-Sekerka predictions, and the other which does not. They claimed that for the class of systems which satisfied Mullins-Sekerka the planar-cellular bifurcation was supercritical and the other subcritical.

In order to make detailed comparison with the predictions from the liner and weakly nonlinear analysis, it is important to have a system where the planar-cellular transition, during directional solidification, is supercritical.

Caroli, Caroli, and Roulet (CCR) [5] predicted that the planar-cellular bifurcation for the moving nematic-isotropic interface of liquid crystals should be supercritical. In addition, this transition occurs in a more convenient region of growth parameters than in usual alloy systems. Oswald *et al.* [6] were the first to observe the planar-cellular transition of the nematic-isotropic interface of a liquid crystal. As predicted by CCR, the transition was observed in a more convenient region of growth parameters and the linear region of the instability (Mullins-Sekerka region) was accessible to observation. Later on, Simon and Libchaber discovered new secondary instabilities in this system, as parity-broken states, traveling waves, solitary modes, and others [7]. It was later demonstrated by Coullet and Ioos [8] that these secondary instabilities are generic in one-dimensional interfaces. By symmetry considerations they predicted the existence of ten different secondary instabilities.

Other experimental advantage of the liquid crystal system is that the characteristic times for dynamic bifurcations are of the order of minutes, while for directional solidification of regular alloys they can be of the order of hours [9,10]. Therefore, by using liquid crystals one can study a wide variety of dynamical phenomena in a reasonable time interval.

The weakly nonlinear analysis of the planar-cellular instability [3,5,11] shows that the time evolution of the amplitude A_k of the most unstable spatial Fourier mode of the interface, with wave vector k, can be described by a third-order Landau-amplitude equation, namely,

$$\frac{dA_k}{dt}=\Omega_k A_k-\alpha_k |A_k|^2 A_k \ , \tag{1}$$

where Ω_k and α_k are real constants. If both Ω_k and α_k are positive, the cellular bifurcation is supercritical; if both are negative, the bifurcation is subcritical. The solution to this equation for the supercritical case is

$$|A_k|=\frac{1}{\sqrt{\alpha_k/\Omega_k+(1/|A_0|^2-\alpha_k/\Omega_k)\exp(-2\Omega_k t)}} \ , \tag{2}$$

where A_0 is the amplitude at $t=0$. The initial perturbation amplitude A_0 originates from thermodynamic fluctuations which are amplified by the instability. The introduction of this initial amplitude is a way of avoiding the introduction of a noise term in the deterministic Landau-amplitude equation above. The drawback is that A_0 is an adjustable parameter in this equation, which is not explicitly connected to more fundamental thermodynamic quantities of the problem.

Experiments on the initial time evolution of a solid-liquid front instability during free growth (driven by heat diffusion) of pure succinonitrile was first performed by Chou and Cummins [12]. In an attempt to compare their results with the predictions of the Mullins-Sekerka linear analysis, some disagreement was found, probably caused by a nonuniform undercooling in front of the interface.

Recently, we performed systematic experiments on the planar-cellular transition of the moving nematic-isotropic interface of the liquid crystal 8CB, during directional solidification [13]. In this case the transition is driven by the diffusion of impurities, resulting in constitutional supercooling of the liquid near the interface. We showed that the amplitude A_k for the cellular bifurcation follows the equation above, with Ω_k and α_k positive real constants, indicating that this bifurcation is supercritical, as anticipated theoretically. In addition, we compare the experimental values for Ω_k and α_k with the theoretical predictions from the two-sided model [5] and from the symmetric model [11]. From the fit of the data of Ω_k as a function of the growth velocity V, for different temperature gradients G, we obtained values for the parameters of the experiment, which are within the range expected for liquid crystals, with one exception: the capillary length, which turned out to be 100 times larger than the predicted value obtained from the ratio between surface tension and latent heat of the nematic-isotropic transition of the liquid crystal 8CB. It indicates that the main restoring force, which stabilizes the nematic-isotropic interface, is not the capillary force originated from the Gibbs-Thomson effect. Therefore, other mechanisms of stabilization of the interface have to be searched. Recently Bechhoefer and Langer [14] considered the elasticity of the nematic phase as a possible stabilizing force for the nematic-isotropic interface. While it reduces the discrepancy, it cannot fully account for the experimental observations. The disagreement between theory and experiment remains unexplained.

In the sections to follow we will describe, in more detail, the experimental method used in our liquid crystal experiments and a comparison of the experimental data obtained with the two-sided model. An analytical calculation of the Eckhaus boundary for this problem, which is general for solidification, will be also presented and it will be compared with the results of the wave vectors of the instability obtained from our experiments.

II. EXPERIMENTAL PROCEDURE

A. Apparatus

Our experimental apparatus is based on the setup designed by Hunt *et al.* [15] and is presented in Fig. 1. It

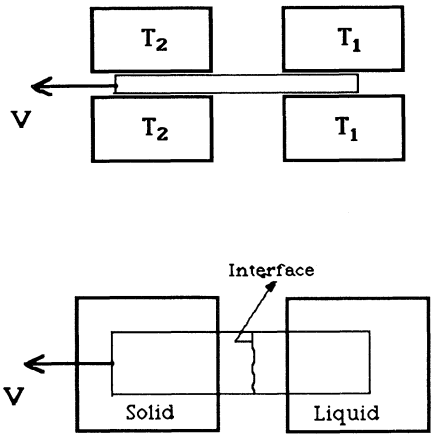

FIG. 1. Experimental apparatus for directional solidification. A temperature gradient G is established on the sample by the hot (T_1) and cold (T_2) ovens. The sample is pulled with velocity V towards the cold oven, such that the ordered phase grows.

consists of two ovens separated by a 10-mm air gap and a precision pulling system. The oven's temperatures are chosen one above and the other below the nematic-isotropic transition temperature of the liquid crystal used. The sample is a layer of liquid crystal, sandwiched between two glass slides, oriented in the homeotropic configuration (the director is normal to the glass slides). The sample is put in contact with the two ovens, such that a temperature gradient is established across it. A nematic-isotropic interface is then formed in the gap between the two ovens. The sample is then pulled at constant speed towards the cold oven and a "directional solidification" process takes place: the nematic phase grows, at the expenses of the isotropic phase, with constant speed that is determined externally by the pulling system. The temperature of the hot oven is controlled by a Ricor temperature controller and the cold one by a Lauda water circulating bath. The overall temperature stability is about 3 cK, during the time of typical experimental runs, which is around $\frac{1}{2}$ h. The pulling system consists of a Micro-Controle micrometric translator, which is coupled to a reduction gear box driven by a dc motor, powered by a stabilized dc power supply. The motor gives an electronic output proportional to its angular speed that can be read by a digital counter and recorded. Careful calibration of the pulling velocity was done by comparing this electronic output with direct readings of the micrometric translator for the various reduction factors of the gear box. Overall stability was better than 0.1% and the accuracy better than 0.1 μm/s.

We use a large field, large working distance Olympus SZ-TR-BR microscope in the configuration of transmitted light, coupled to a Dage-MTI-CCD camera (480 lines $\times$ 640 horizontal pixels). Images were recorded with a Sony Hi8 VCR, EVO-9650. Recording is digitially indexed in the tape, such that the time resolution is exactly one frame or $\frac{1}{30}$ s. Later, recorded images are digitized using a Data Translation frame grabber DT2255 and stored on a Mackintosh Quadra 700 computer. They are processed and the interface extracted. The contrast of the interface images was always very good, such that digital filtering or the use of polarizers was unnecessary. Lengths in the sample were calibrated by using a microruler, with a 2-mm scale and 200 divisions. Before each experimental run, an image of the ruler was taken to calibrate the lengths involved. This procedure gives us reliable length measurements, independently of the optical magnification used. The measured Nyquist wave vector was typically 2.18 μm^{-1}.

B. Sample preparation

We used the liquid crystal 8CB (4,4'-*n*-octylcyanobiphenyl) made by BHD Ltd. [16]. It is a thermotropic liquid crystal whose characteristics of chemical stability and physicochemical properties make it convenient for directional solidification experiments. The temperature of the nematic-isotropic transition is 40.5 °C and 33.5 °C for the smectic-A–nematic one, both for a pure material. Table I gives the values of some of its physicochemical constants. According to the manufacturer, the main impurity content of the material, as it leaves the factory, is water with saturation concentration of 0.15 mol % [16], mainly due to the highly hygroscope isotro-

TABLE I. Thermodynamic data for the liquid crystal 8CB.

Transition	Transition temperatures T (°C)	Reference
Sol→Sm-A[a]	21.5	16
Sm-A→N	33.5	16
N→I	40.5	16

	Physicochemical properties Value	Units	Reference
Mol. weight	291.2	g/mol	16
Density	0.980	g/cm^3	19[b]
L_1[c]	1.2×10^{-7}	dyn	19[b]
L_2	1.9×10^{-7}	dyn	19[b]
L_3	2.4×10^{-7}	dyn	19[b]
Viscosity	3.0×10^{-2}	poise	19[b]
MWC[d]	0.15	mol %	16

	Nematic-isotropic transition Value	Units	Reference
Surface tension	0.0094	dyn/cm	19
Latent heat	6.12×10^9	erg/mol	19
1st Landau coef.	1.9×10^6	erg/(cm^{3}K)	19
Correlat. length	$17.5\pm^{18}_{10}$	Å	19
T_{NI}-T^*[e]	2	K	19

[a]Sm-A denotes smectic A.
[b]Values measured at the $N\rightarrow I$ transition.
[c]Franck elastic constants.
[d]MWC denotes maximum water concentration.
[e]T^* denotes the virtual second-order transition temperature.

pic phase. During sample preparation no special care was taken to control the water content in the material. As a consequence, the impurity and its concentration are unknown parameters of the experiment. The glass plates are first cleaned with a solution of distilled water and Extran [17] at 60 °C in an ultrasound bath for 30 min. After that, they were extensively rinsed with running distilled water and dried at 120 °C for 4 h.

To generate the homeotropic configuration, the glass plates were covered by a silane agent [18] composed of molecules with a silane base and a long carbonic chain (like $C_{18}H_{38}$), which form a tail parallel or perpendicular to the glass substrate, and gives rise to a planar (LC molecules parallel to the substrate) or a homeotropic configuration, depending on the orientation of the chain relative to the silane base. Two microscope glass slides, treated with silane and separated by a spacer of a few micrometers, form the cell where the LC is introduced in the isotropic phase. The carbonic tail of the silane causes a good homeotropic orientation for spacer thickness of the order of or less than 50 μm. The samples were prepared open to the atmosphere, and since the isotropic phase is highly hygroscope, no control of the water content was possible.

In Ref. [19] convective rolls in front of the interface were observed for sample thickness greater than 5 μm. To avoid this effect, which can complicate the theoretical analysis of the experiment, we constructed our sample in an edgelike shape, such that in one end the glass plates touch each other, and at the other end a spacer of 20 μm was used. The sample thickness then varies from zero on one end up to 20 μm at the other end. The experiments were performed in a working region of the sample where the thickness varied at most from 2.5 up to 4.5 μm. By knowing the spacer thickness, which was measured with a digital Mytutoyo micrometer with precision of 1 μm, and using interference techniques, the thickness of the sample was measured with approximately 5% error. To select the glass plates with the best flatness, each one is first checked against an optical flat ($\lambda/20$) by using a laser interference technique. With the chosen plates, a different interference pattern is constructed with two plates in contact with each other, without a spacer. Again, the best combination of two plates is then chosen. At this point, the edgelike cell is prepared and the working region is delimited. After that, the cell is filled in with the liquid crystal. All the experiments were performed within the working region, generally measuring 15×17 mm^2.

C. Measurements

In our experiments we were able to follow the time evolution of the nematic-isotropic interface morphology. Images of an interface at various instant of time are shown in Fig. 2. The images are processed and the interface positions are extracted. We perform fast Fourier transforms (FFT) of the interfaces and obtain the spatial power spectra of the interface deformations, as shown in Fig. 3(a). Finally, the value of the magnitude of the amplitude A_k as a function of the time is obtained. An ex-

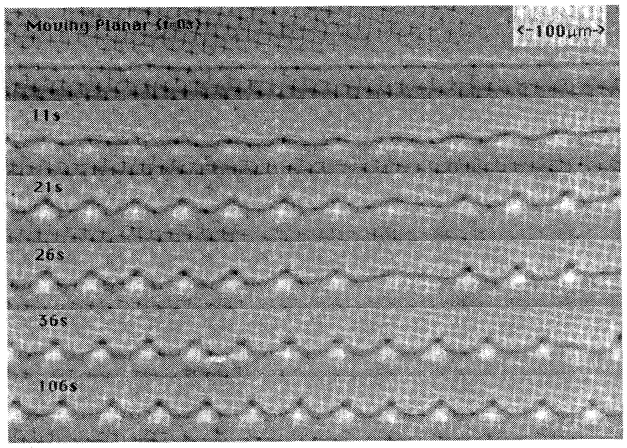

FIG. 2. Sequence of images showing the interface at different times. The nematic phase is above and the isotropic one is below the interface. Experiment performed with $G = 43.3$ K/cm and $V = 18.5$ μm/s.

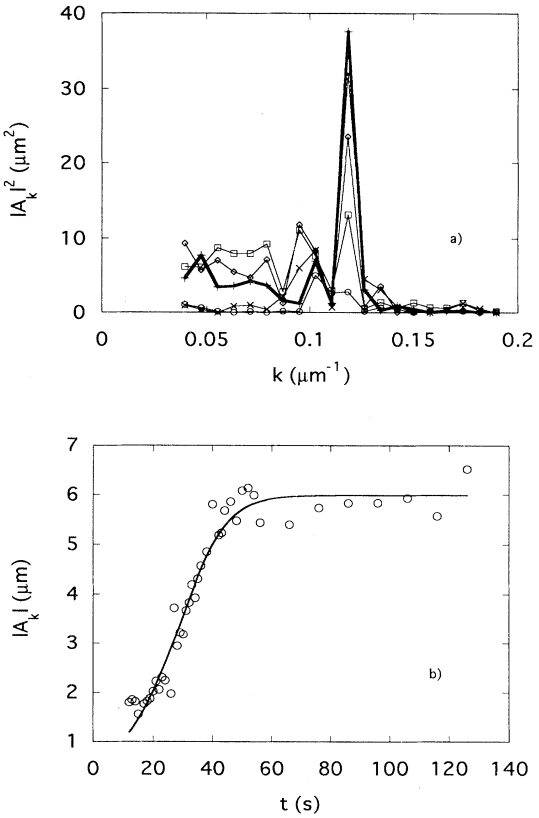

FIG. 3. (a) Power spectra for the sequence shown in Fig. 2. The thickest line refers to the latest time ($t = 106$ s in Fig. 2). (b) Time evolution for the amplitude of the most unstable mode obtained from the power spectra of (a). The solid line is the best fit using Eq. (2). For this fit $\Omega_k = 0.069$ s^{-1} and $\alpha_k = 0.002$ (μm^2 s)$^{-1}$.

ample for $V=18.5\ \mu$m/s and $G=43.3$ K/cm is shown in Fig. 3(b). The circles are the experimental points and the continuous line is the fit using Eq. (2). We see that the time evolution of the nematic-isotropic deformations during directional solidification follows the universal behavior described by a Landau-amplitude equation. From this fit we obtain the values for Ω_k and α_k for different V and G. These values will be compared with solidification models.

III. THE TWO-SIDED MODEL OF SOLIDIFICATION

A. Theory of CCR

In this section we present the relevant results of a model of directional solidification from the work by CCR [5]. This model considers that thermal and impurity diffusion take place in both sides of the interface. In addition, the calculations are done for any segregation coefficient K. Consequently, the two-sided model has both the one-sided [2,3] and the symmetric [11] models as limiting cases.

In the sketch of the directional solidification setup presented in Fig. 1, the sample is put in thermal contact with the ovens at constant temperatures $T_1 > T_M$ (the liquid side) and $T_2 < T_M$ (the solid side). Here T_M is the melting temperature of a crystal or the nematic-isotropic transition temperature of our liquid crystal. A stationary temperature gradient G is established along the sample and a planar interface at $T=T_M$ is formed. The sample is then pulled at constant velocity V. If a small concentration C_0 of an impurity is dissolved into the material, a cellular instability may occur for some values of the pair (G,V). The basic equations for describing this phenomenon are stated below.

(a) Volume diffusion of concentration and heat in each phase:

$$D\nabla^2 C + V\frac{\partial C}{\partial z} - \frac{\partial C}{\partial t} = 0 , \tag{3a}$$

$$\nabla^2 T = 0 , \tag{3b}$$

$$D'\nabla^2 C' + V\frac{\partial C'}{\partial z} - \frac{\partial C'}{\partial t} = 0 , \tag{3c}$$

$$\nabla^2 T' = 0 . \tag{3d}$$

Equations (3a) and (3b) are defined for the liquid phase, while Eqs. (3c) and (3d) are defined for the solid phase. Equations (3b) and (3d) are used, rather than the full diffusion equation because heat diffusion coefficients are of the order of 10^3 larger than mass diffusion coefficients, such that the thermal fields can be considered static during the time scale of variations of the concentration fields.

(b) Interface boundary conditions, at $z=\varepsilon\zeta(x,t)$, where ε is a smallness parameter ($\varepsilon=0$ corresponds to a planar interface): continuity of temperature,

$$T = T' ; \tag{4a}$$

heat balance,

$$n\frac{\partial T'}{\partial z} - \frac{\partial T}{\partial z} - \varepsilon\frac{\partial \zeta}{\partial x}\left[n\frac{\partial T'}{\partial x} - \frac{\partial T}{\partial x} \right] = 0 ; \tag{4b}$$

local phase equilibrium,

$$C' = KC ; \tag{4c}$$

mass conservation,

$$\frac{\partial C}{\partial z} - \eta\frac{\partial C'}{\partial z} - \varepsilon\frac{\partial \zeta}{\partial x}\left[\frac{\partial C}{\partial x} - \eta\frac{\partial C'}{\partial x} \right] = \frac{(K-1)\left[V + \varepsilon\frac{\partial \zeta}{\partial t} \right] C}{D} ; \tag{4d}$$

curvature-induced local-interface-temperature shift,

$$T = T_M\left\{ 1 + \frac{mC}{T_M} + d_0\varepsilon\frac{\partial^2 \zeta}{\partial x^2}\left[1+\varepsilon^2\left[\frac{\partial \zeta}{\partial x} \right]^2 \right]^{-3/2} \right\} ; \tag{4e}$$

where $\eta=D'/D$, D and D' are the impurity diffusion coefficients, and $n=\mathcal{K}/\mathcal{K}'$, with $\mathcal{K}$ and $\mathcal{K}'$ the thermal conductivities; primed variables refer to the solid phase and the unprimed ones to the liquid phase; d_0 is the capillary length, given by the ratio between the solid-liquid (nematic-isotropic) surface tension and the latent heat; m is the liquidus slope of the binary phase diagram, and it is a negative quantity for the systems considered here. In the heat balance equation, Eq. (4b), we have neglected the latent heat, since it is very small for the nematic-isotropic transition.

In their work, CCR first obtained the solution for the concentration and thermal fields for the stationary planar interface. They studied the stability of this solution by perturbing the planar-interface morphology with a small deformation, with a single spatial frequency k, as below:

$$\zeta(x,t) = \exp(\Omega_k t)\cos(kx) .$$

The temperature and concentration fields were perturbed in a similar manner. There are six unknowns: the fields in both phases, Ω_k and k, and five thermodynamic boundary conditions at the interface. We use them to eliminate the four fields and get a relation between Ω_k and k. To first order in ε, CCR obtained a dispersion relation as a function of the control parameters G, V, and C_0 given by

$$\Omega\tau = \left[1 + \frac{2Gl}{(n+1)(1-K)mC_0} + \frac{T_M d_0 l k^2}{(1-K)mC_0} \right]\{p(\Omega,k) - 1 + K[1+\eta p'(\Omega,k)]\} - K[1+\eta p'(\Omega,k)] , \tag{5a}$$

where $l=D/V, \tau=l/V$, and

$$p(\Omega,k)=\tfrac{1}{2}+\sqrt{\tfrac{1}{4}+\Omega\tau(kl)^2}\ ,$$

$$p'(\Omega,k)=\frac{-1}{2\eta}+\frac{1}{\eta}\sqrt{\tfrac{1}{4}+\eta\Omega\tau+(\eta kl)^2}\ .$$

In the quasistationary approximation $\Omega\tau \ll (kl)^2$, such that $\Omega\tau$ can be neglected inside the expressions for p and p' above. The condition $\Omega\tau \ll (kl)^2$ can be rewritten as $\Omega \ll k^2 D$. For our experimental data, the worse situation corresponds to $k^2 D \sim 0.9\ \mathrm{s}^{-1}$ and $\Omega = 0.17\ \mathrm{s}^{-1}$, such that for the analysis of our results presented in this paper, this approximation is quite adequate.

As in the traditional Mullins-Sekerka analysis, for a given G and C_0, there is a critical pulling velocity V_c such that the interface's morphology is stable for all k. For V greater than V_c a continuous finite band of unstable wave vectors is allowed. This band ends at a second velocity, V_R, where capillary effects reestablish the planar interface. The Mullins-Sekerka neutral stability curve is indicated in Fig. 4, by the continuous line. Since no single mode is selected the question of pattern selection is not resolved.

For thin samples, where the heat transport is defined by the sample's boundaries (like glass slides), or for materials with similar thermal diffusivities in the ordered and disordered phases, we can set $n=1$. Thin samples of liquid crystals meet both requirements so we assume $n=1$ as a good approximation in our work.

CCR performed also a nonlinear series perturbation owing to obtaining the cubic coefficient of the third-order Landau-amplitude equation. For this, following WS [3], they assumed that the fields and the interface position can be expanded as

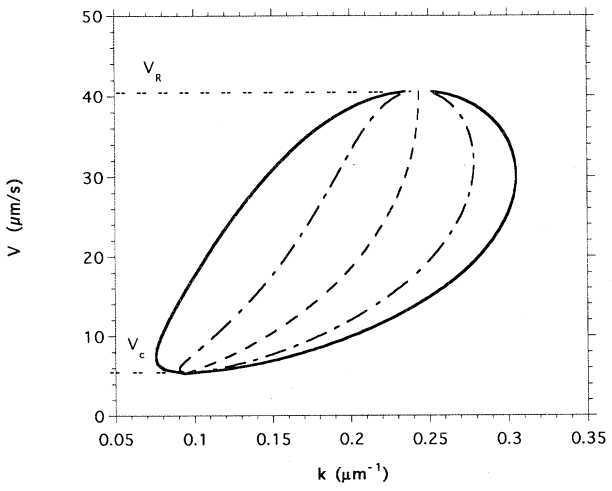

FIG. 4. Mullins-Sekerka stability region on the V-K plane. The continuous line is the Mullins-Sekerka neutral curve, the dash-dotted line is the calculated Eckhaus boundary, and the dashed line represents the wave vectors with highest growth rates obtained from the linear analysis.

$$\varepsilon\zeta(x,t;\varepsilon)=\sum_{n=1}^{\infty}\varepsilon^n\zeta_n(x,t)\ ,$$

$$\mathbf{v}(x,t)=\sum_{n=1}^{\infty}\varepsilon^n\mathbf{v}_n(x,t)\ ,$$

where $\mathbf{v}(x,z,t)=(C,C',T,T')$, $\zeta_1(x,t)=A(t)\cos(kx)$, and $\mathbf{v}_1(x,z,t)=A(t)\mathbf{v}_{11}(z)\cos(kx)$ with $\mathbf{v}_{11}(z)$ to be determined.

The first-order term of these expansions gives the linear stability results. The nonlinear terms present in the boundary conditions [Eqs. (4a)–(4e)] give rise to harmonics of the single mode considered in the linear analysis. Sufficiently near the bifurcation, where a narrow band of modes is unstable, we can assume that those harmonics are not active. Collecting terms in the above expansion up to second order in ε, CCR obtained a third-order amplitude equation [Eq. (1)]. The cubic coefficient α_k is algebraically very complex and will not be displayed here. It can be found in the appendix of the work of CCR.

B. Kinetic effects

If the crystal-melt interface is rough on atomic scale, the kinetic growth law for solidification is given by

$$V=\mu\Delta T\ ,$$

where V is the growth velocity, μ is the kinetic coefficient, and ΔT is the undercooling of the interface. With the addition of kinetics the boundary condition Eq. (4e) has to be modified, since the local temperature of the interface is smaller than the melting temperature to keep the crystal growing at velocity V. The new boundary condition is then

$$T=T_M\left[1+\frac{mC}{T_M}+d_0\varepsilon\frac{\partial^2\zeta}{\partial x^2}\left[1+\varepsilon^2\left[\frac{\partial\zeta}{\partial x}\right]^2\right]^{-3/2}-\frac{V+\frac{\partial\zeta}{\partial t}}{\mu T_M}\right]\ . \tag{4e'}$$

If we redo the calculations of CCR, but with the boundary condition given by Eq. (4e'), we obtain

$$\Omega(\mu)=\Omega\left[1-\frac{p+K-1+\eta p'}{mG_C\mu\tau}\right]^{-1}\ , \tag{5b}$$

where $G_c=(1-K)C_0/Kl$, and all the other variables have been defined previously. We see that for very fast kinetics, i.e., μ very large, Eq. (5b) reduces to Eq. (5a), since, in this case, the temperature of the interface is very close to the equilibrium temperature, and kinetic effects would be unimportant. If $\eta=0$, which corresponds to the one-sided model, Eq. (5b) reduces to the solution of Coriell and Sekerka [20], for the one-sided model with kinetics effects included. Equation (5b) is a generalization for the two-sided model.

C. Experimental results and analysis

Our main aim, in this section, is to test the two-sided model of solidification, which should be adequate for the liquid crystal system. All the data, presented in this paper, were obtained with the same sample, for different combinations of V and G, as indicated in Table II.

The temperatures of the furnaces are chosen to give the desired value of G. After stabilization of these temperatures the liquid crystal sample is introduced in the apparatus. By keeping the pulling velocity equal to zero, after a while, a still, clean, flat nematic-isotropic interface is seen in the field of view of the microscope. We then set the desired pulling velocity V and videotape the motion of the interface. The planar interface moves towards the cold end of the furnace and stops at another position. The characteristic times for this initial transient can be a few seconds up to several minutes. It is larger for smaller velocities as one would expect. As we increase the velocity, the new position of the interface is farther away from the initial one, since a larger undercooling of the isotropic phase is necessary for keeping higher growth rates. By another method of measurement we studied the kinetics of this planar nematic-isotropic interface. We obtained that the nematic-isotropic interface behaves like a rough crystal-melt interface with a linear kinetic law:

$$V=\mu\Delta T \ ,$$

where μ is the kinetic coefficient and ΔT is the undercooling of the interface. The measured kinetic coefficient is

$$\mu=220\pm20 \ \mu\text{m}/(\text{s K}) \ .$$

We will analyze our data both with and without kinetic effects included.

During the motion of the planar interface reported above, a planar-cellular morphological instability may develop, for some combinations of G and V. The images from the time evolution of the cellular interface are recorded and the time resolution of one frame ($\frac{1}{30}$ s) was sufficient for the region of parameters (G,V) used in these experiments. After extracting the coordinates of the interface by digital analysis of the images, we perform a FFT (fast Fourier transform) of the interface for different times and obtain the spatial Fourier components A_k of the interface deformations as a function of time. As we mentioned before, the transformation from pixels unit to length units is obtained from the image of a calibrated ruler taken under the same optical conditions as the images of the interface.

TABLE II. Values for the control parameters G and V used in our experiments. The boldfaced numbers were used to obtain the quantitative data reported in this paper.

G (K/cm)	V (μm/s)
15	1.0,2.0,4.0,5.5,7.0, 8.5,10.0
20	1.5,2.0,3.0,4.0,5.0, 6.9.8.6,10.3
25	**2.0,3.0,4.0,5.7,7.5, 9.2,10.9**
30	2.3,**3.4**,4.6,5.2,5.7, 6.9,8.0,9.7,11.5
35	**5.7,6.3,6.9,7.5,8.0, 10.3,12.6,14.3**
43.3	**5.2,6.3,7.2,8.0,10.0, 14.3,18.5,22.5**

For checking the two-sided model of CCR we look for a region of parameters (V,G), where the observed dynamics of the interface was simple enough to be described by a third-order Landau-amplitude equation. This restricted the parameter region for the sample used to 15 K/cm $< G <$ 50 K/cm and $\varepsilon=(V-V_c)/V_c<5$, knowing that V_c depends on G. For $G<15$ K/cm, even for pulling velocities near V_c, the behavior of the interface was very complex with, at long times, the appearance of spatio-temporal chaos, as reported previously by Flesselles *et al.* [9]. For larger values of G and for $\varepsilon>5$ the cellular pattern has deep grooves similar to the case of crystal-melt interfaces, and very fast initial-instability growth rates. The power spectra contained many spatial components and there was no predominance of a particular mode for all times. In Table II, the values of V and G used to obtain the quantitative data reported in this paper are presented as bold-faced numbers. For these parameters, we did not observe the presence of significant contributions of higher spatial harmonics in the spectra of the cellular pattern. In most cases the spatial Fourier amplitude A_k grows exponentially and saturates, as one would expect for a cellular pattern. However, in some cases, after saturation for a long time, A_k starts to grow again and the interface starts to have a more complex dynamic behavior. We do not know if this is an intrinsic phenomenon in this system, or an effect due to the finite size of the sample. We are presently investigating it. Consequently, we will use in this analysis only the data with a saturation time which lasted at least three times longer than the time constant of the initial exponential growth of A_k.

A typical plot of the magnitude of A_k as function of time is shown in Fig. 3(b). The open circles are the experimental points and the continuous curve is the fit using the solution of the third-order Landau-amplitude equation, Eq. (2). From this fit one obtains the instability growth rate Ω_k and the cubic coefficient α_k.

In order to compare the experimental values of Ω_k and α_k with the predictions of the two-sided model, we use a relation between the (equilibrium) segregation coefficient K and the liquidus slope m for diluted mixtures, the well-known van t'Hoff formula [21]

$$m=-\frac{RT_M^2}{L}(1-K) \ , \tag{6}$$

where R is the universal gas constant and L the latent heat. For the analysis of our experimental data we substitute Eq. (6) into Eqs. (5a) and (5b), such that the growth rates depend only on the parameter K instead of the pair m and K. Therefore, during the fitting procedure using Eqs. (5a) and (5b) the adjustable parameters are D, K, C_0, and d_0.

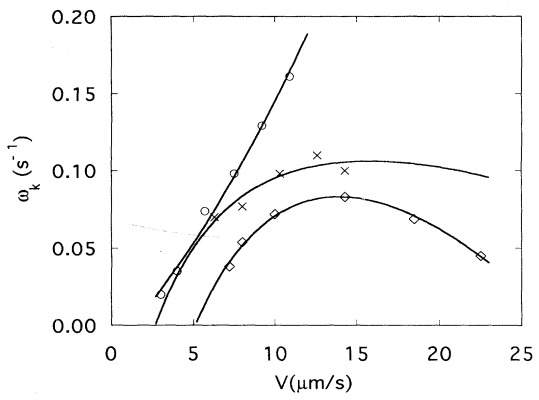

FIG. 5. Best fits of Eq. (5b) to the set of data of growth rates Ω_k, for three different temperature gradients (solid lines), and for $\eta=0.5$. Symbols are the experimental points. Temperature gradients are $G=43.3$ K/cm ($\Diamond$), 35 K/cm ($\times$), and 25 K/cm ($\circ$). Parameters from these fits are displayed in Table III.

In Fig. 5 we present the data of Ω_k (including kinetic effects) for different pulling velocities V and temperature gradients G. The continuous curves are the fittings using Eq. (5b) from the two-sided model with kinetics, for $\mu=220$ μm/sK and $\eta=0.5$. Since the linear and weakly nonlinear analysis of solidification models do not predict wave-vector selection, in order to fit Eqs. (5a) and (5b) to the experimental data, we used our experimental values for the wave vector k. Both equations fit the data very well. The fitting parameters can be seen in Table III. Kinetic effects caused minor changes in these parameters. In addition, these results do not change significantly for values of η in the range from 0.4 up to 0.6. Therefore, we have used $\eta=0.5$, which is the experimental value for various impurities in 8CB [19]. The value obtained $C_0=0.15$ mol% is consistent with the hypothesis that the main impurity is water. The value $D\sim 70$ $\mu m^2/s$, for the diffusion coefficient of the impurity in the isotropic phase, is also reasonable, if we compare with reported values for D for methyl blue in the isotropic phase of 8CB, which are of the order of 40 $\mu m^2/s$ [22]. Since the water molecule is smaller than the methyl blue molecule, this result is also consistent with the hypothesis that water is the main impurity. The values from 0.70 up to 0.74, for the segregation coefficient K, are also in the range of measured values of K for many impurities, for the nematic-isotropic transition in 8CB. Finally, the value $d_0\sim 7$ Å, for the capillary length, is the only one which does not agree with the two-sided model. As seen in the preceding section, the capillary length is the result of the ratio between the surface tension and the latent heat for the nematic-isotropic interface. From tabulated values for these quantities one obtains that the capillary length should be of the order of 0.05 Å. Recently, Bechhoefer and Langer [14] took into account the elastic energy for deforming the nematic phase, as an extra stabilizing energy for the nematic-isotropic interface. Even though this calculation of the capillary length has increased its value, it was not enough to solve the overall discrepancy.

The coupling between anisotropic impurity diffusion in the nematic phase and elastic deformations of the interface was recently considered by Misbah and Valance [24]. By solving the two-sided model, but considering the director dynamics and its coupling with the diffusion field in the nematic phase (both in the bulk and at the interface), they showed that the Mullins-Sekerka instability presents, in this case, a growth rate with real and imaginary parts. The presence of an imaginary part in the growth rate should manifest itself by a drift of the structure transversely to the front. Even though this analysis predicts new effects during melting and growth of the nematic phase, it does not seem to be relevant to explain the unusual capillary length that we observed in our experiments. Therefore, a plausible mechanism, or mechanisms, for explaining quantitatively the stabilization of the nematic-isotropic interface in the sort of experiments performed here, are still lacking.

The values, obtained from the fittings for the cubic coefficient α_k, showed large error bars. Nevertheless, these values are compatible with the values predicted by the two-sided and symmetric models, for the parameters C_0, d_0, K, and D obtained from the linear analysis presented before. See our Ref. [13] for a complete set of values of the cubic coefficient α_k, for different pairs (G,V).

TABLE III. Rows refer to the fitting parameters of Eqs. (5a) and (5b) to the data of Ω_k. Values in parentheses refer to Eq. (5b), where kinetic effects are included. Values marked with an asterisk are fixed in the fitting.

Data set (K/cm)	D ($\mu m^2/s$)	K	C_0 (mol %)	d_0 (Å)
$G=43.4$	67±2	0.740±0.004	0.14±0.02	6±2
	(70±1)	(0.740±0.004)	(0.15±0.03)	(7.5±2)
$G=35.0$	67±5	0.719±0.004	0.14*	6*
	(70±4)	(0.722±0.004)	0.15*	7.5*
$G=25.0$	66±6	0.690±0.01	0.14*	6*
	(72±3)	(0.720±0.004)	0.15*	7.5*

IV. ECKHAUS INSTABILITY

A. Analytical calculation of the Eckhaus boundary for directional solidification

The Eckhaus instability arises when a one-mode pattern whose amplitude follows Eq. (1) is unstable against small perturbations on its phase [25]. This is a classical secondary instability first studied in the context of hydrodynamics [26]. The classical result given by Eckhaus [27], valid near the bifurcation shows the existence of a small band, inside the linearly unstable one, for which the original pattern is stable against phase perturbations. The first experimental measurement of the space and time evolution of an Eckhaus instability was performed by Lowe *et al.* [28] on experiments of electrohydrodynamics in liquid crystals. It is believed that, since this instability shrinks the allowed band of wave vectors, it can be an important mechanism of pattern selection. More recently, in experiments on directional solidification in liquid crystals, Simon, Bechhoefer, and Libchaber [29] have seen evidence for the Eckhaus instability on the high wave number region of the Eckhaus band, and a number of other secondary instabilities (see also Ref. [7]). The work of Hernández-García *et al.* [30] predicts that thermal fluctuations can be sufficiently strong to drive the phase instability of unstable patterns. Misbah and co-workers [31,32] developed numerical calculations of secondary instabilities using the symmetric model for directional solidification and not restricted to regions of the parameter space near the bifurcation. In particular, they found that the Eckhaus boundary is asymmetric for wave vectors around the critical one. This tilted Eckhaus boundary was not found previously in the classical calculations using an amplitude equation. Therefore, these numerical calculations were very important to obtain a correct Eckhaus boundary for solification problems.

In this section we present an analytical calculation of the Eckhaus boundary valid over all the linearly unstable band, and for any region of the parameter space. We also obtain a tilted Eckhaus band, but from an amplitude equation. Contrary to the conclusions of Brattkus and Misbah [32], we think that this tilting is caused by the properties of the linear dispersion curve and not due to strong nonlinear interactions of a great quantity of different spatial modes.

In our derivation some requirements on the dispersion curve are assumed, but they are sufficiently general to be model independent.

We start from a single mode pattern,

$$\zeta_k(x,t)=a_k(t)e^{ikx}+\text{c.c.} , \tag{7}$$

where $a_k(t)$ is the mode amplitude, $\zeta_k(x,t)$ is the pattern that is a real function of space and time variables, and c.c. stands for complex conjugate. Assume that each mode amplitude satisfies a third-order Landau-amplitude equation

$$\frac{da_k}{dt}=\Omega(k,\varepsilon)a_k-\alpha(k,\varepsilon)|a_k|^2a_k \tag{8}$$

with $\Omega(k,\varepsilon)$ the growth rate of the mode k obtained from the linear stability analysis of the original problem and ε is a control parameter, which is zero at the planar-cellular bifurcation. A more complex pattern, with many modes interacting during their time evolution, is given by

$$U(x,t)=\sum_k \zeta_k(x,t) , \tag{9}$$

which no longer follows the time evolution defined by Eq. (8), since nonlinear interactions cause the superposition principle to fail. Nevertheless, mode couplings that lead to the same original k are possible [25,26] with

$$k=(k-k_1+k_2)+(k_1)-(k_2) ,$$

which corresponds to a third-order term of the form

$$\sum_{k_1k_2} a_{k_1}e^{ik_1x}a^*_{k_2}e^{-ik_2x}a_{k-k_1+k_2}e^{i(k-k_1+k_2)x}$$

$$=e^{ikx}\sum_{k_1k_2} a_{k_1}a^*_{k_2}a_{k-k_1+k_2} .$$

It follows that the time evolution of the pattern given by Eq. (9) is

$$\frac{\partial U}{\partial t}=\sum_k \left[\Omega(k,\varepsilon)a_ke^{ikx} -\alpha(k,\varepsilon)e^{ikx}\sum_{k_1k_2} a_{k_1}a^*_{k_2}a_{k-k_1+k_2}\right]+\text{c.c.} \tag{10}$$

If k_0 is a basic mode of $U(x,t)$, it is convenient to write $k=k_0+q$, replace $\sum_k \rightarrow \sum_q$, and define the (complex) amplitude of the pattern by

$$A(x,t)=\sum_q a_q(t)e^{iqx} , \tag{11}$$

which satisfies, after substitution into Eq. (10),

$$\frac{\partial A}{\partial t}=\sum_q \Omega(k_0+q,\varepsilon)a_qe^{iqx}-\alpha(k_0,\varepsilon)|A|^2A . \tag{12}$$

For the purpose of this work, we assume, in the above equation, that the spectrum of the pattern consists of a small wave packet around k_0, in such a way that for a given k_0, α is constant for any value of the control parameter, i.e., $\alpha(k_0+q,\varepsilon)\approx\alpha(k_0,\varepsilon)$. At the latest step of our reasoning q will be made arbitrarily small, so no serious restriction is imposed on this parameter. We also assume a dispersion relation of a general form like in Fig. 6. This form can represent instabilities in which the homogeneous solution of a pattern is unstable above a certain critical value of the control parameter. It is worthwhile to stress the explicit dependence of Ω on k^2 coming from the reflection symmetry $x\rightarrow -x$ for infinite systems. Expanding Ω about k_0^2 we obtain

$$\Omega[(k_0+q)^2]=\Omega_0+Bq-Cq^2+O(q^3) \tag{13}$$

with $\Omega_0=\Omega(k_0)$, $B=2[d\Omega/d(k_0^2)]k_0$, and C

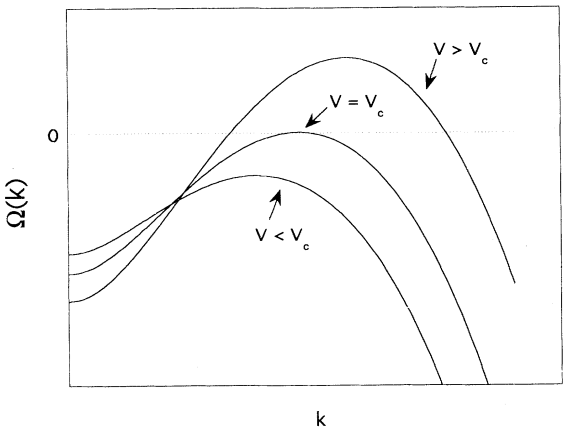

FIG. 6. Typical dispersion curves $\Omega(k)$ used in our calculation of the Eckhaus band. These curves are characteristic to many pattern-forming systems. V is a control parameter.

$=-[2k_0^2 d^2\Omega/d(k_0^2)^2+d\Omega/d(k_0^2)]$. Introducing Eq. (13) into Eq. (12) we obtain, up to second order,

$$\frac{\partial A}{\partial t}=\Omega_0 A-iB\frac{\partial A}{\partial x}+C\frac{\partial^2 A}{\partial x^2}-\alpha|A|^2 A \ . \tag{14}$$

The above equation defines an amplitude equation for the wave packet, that is valid for any k_0 and ε. A real, homogeneous, and stationary solution of it is $A_0=\sqrt{(\Omega_0/\alpha)}$, whose associated pattern is $U_0(x)=2\sqrt{(\Omega_0/\alpha)}\cos(k_0 x)$. We test the stability of this solution by perturbing it with a small complex amplitude $y(x,t)$. By introducing $y(x,t)$ into Eq. (14) and keeping only the linear terms in $y(x,t)$, one obtains

$$\frac{\partial y}{\partial t}=-iB\frac{\partial y}{\partial x}+C\frac{\partial^2 y}{\partial x^2}-\Omega_0(y+y^*) \ . \tag{15}$$

Now, consider a perturbation described by a long wavelength modulation of the stationary amplitude A_0 and compatible with the expansion defined in Eq. (13), i.e., with $q \ll k_0$,

$$y(x,t)=Ze^{\omega t}\cos(qx)+iVe^{\omega t}\sin(qx) \ , \tag{16}$$

where Z and V are real numbers. Introducing it into Eq. (15) we obtain a system of two linear equations for Z and V, whose solvability condition is given by

$$\omega^2+2(Cq^2+\Omega_0)\omega+C^2q^4+(2\Omega_0 C-B^2)q^2=0 \ . \tag{17}$$

For small q the roots of the above equation are

$$\omega(q^2)_+=\left\{2k_0^2\left[\frac{\partial^2\Omega}{\partial(k_0^2)^2}+\frac{1}{\Omega_0}\left[\frac{\partial\Omega}{\partial(k_0^2)}\right]^2\right]+\frac{\partial\Omega}{\partial(k_0^2)}\right\}q^2 \ , \tag{18a}$$

$$\omega(q^2)_-=\left\{2k_0^2\left[\frac{\partial^2\Omega}{\partial(k_0^2)^2}-\frac{1}{\Omega_0}\left[\frac{\partial\Omega}{\partial(k_0^2)}\right]^2\right]+\frac{\partial\Omega}{\partial(k_0^2)}\right\}q^2-\Omega_0 \ . \tag{18b}$$

We see that for $q=0$, $\omega_+=0$, and $\omega_-=-\Omega_0$. Thus, $\omega_+(0)$ corresponds to a neutral mode, which in the present case is a phase mode, since a shift in the overall phase of the pattern leaves the pattern unchanged. $\omega_-(0)$ corresponds to an amplitude mode, since if we disturb the amplitude of the cellular pattern it will relax back with a rate Ω_0 [25].

For $q\neq 0$ the system is Eckhaus unstable if $\omega_+>0$, so $\omega_+=0$ defines the Eckhaus boundary. From Eq. (18b) we see that $\omega_-<0$ for sufficiently small q, such that the amplitude of the pattern is always stable in this approximation. The equation for ω_+ shows that this system can undergo a phase instability with a diffusive behavior ($\omega_+\sim Dq^2$), with a phase diffusion coefficient given by

$$D(k^2,\varepsilon)=-\left\{2k^2\left[\frac{\partial^2\Omega}{\partial(k^2)^2}+\frac{1}{\Omega}\left[\frac{\partial\Omega}{\partial(k^2)}\right]^2\right]+\frac{\partial\Omega}{\partial(k^2)}\right\} \tag{19}$$

with no subscripts, since the reference point k_0 is arbitrary. The zeros of this coefficient give the Eckhaus boundary compatible with the general amplitude equation, Eq. (1), and the general dispersion relation of Fig. 6. As stressed above, this result is not restricted to regions near the bifurcation, as it is in the traditional calculations. As we will see below, the third term in Eq. (19), $d\Omega/d(k^2)$, is the nontraditional one and it is responsible for the tilting of the Eckhaus boundary.

Analytical determination of the Eckhaus boundary is, in principle, obtained by inverting the implicit equation $D(k^2,\varepsilon)=0$. To determine the Eckhaus boundary for the two-sided model we substitute the dispersion relation given by Eq. (5b) into Eq. (19) and solve $D(k^2,\varepsilon)=0$ numerically, since an analytical expression in this case is not possible. An example, using the parameters of our experiments obtained from the linear analysis, for $G=43.3$ K/cm, $K=0.74$, $D=70$ $\mu m^2/s$, $C_0=0.15$ mol%, and $d_0=7.5$ Å, is shown in Fig. 4. The continuous line represents the linear-neutral-stability curve. The trace-dotted line represents the Eckhaus boundary and the dashed line the maximum-growth-rate wave vector.

Our Fig. 4 is qualitatively similar to Fig. 5 from the numerical work of Gazali and Misbah of Ref. [31]. In that paper, the obtained tilted Eckhaus boundary was supposed to be due to strong interactions between many modes. In our derivation, this effect can be attributed to the fact that the linear dispersion relation is asymmetric, given that $\Omega[(k_0+q)^2,\varepsilon]\neq\Omega[(k_0-q)^2,\varepsilon]$ for arbitrary k_0 and ε. This restriction generates the linear dependence on the first derivative of Ω in relation to k^2, as can be seen in Eq. (19), but only few modes, nearly located, interact to originate this phase instability.

As expected, near the bifurcation, an analytical expression for the phase diffusion coefficient can be obtained.

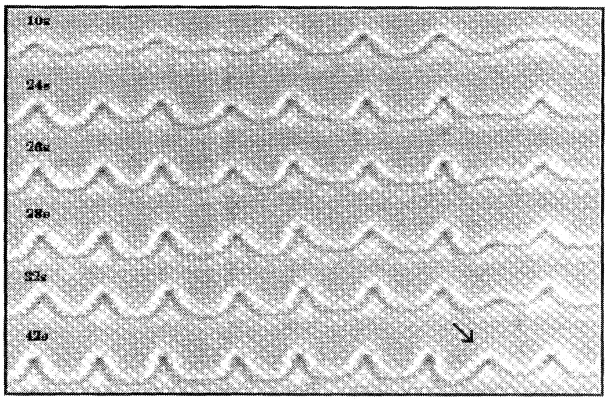

FIG. 7. Sequence of images showing the birth of a new cell during the time evolution of the interface's morphology. Experiment performed at $G=25$ K/cm and $V=5.7$ μm/s.

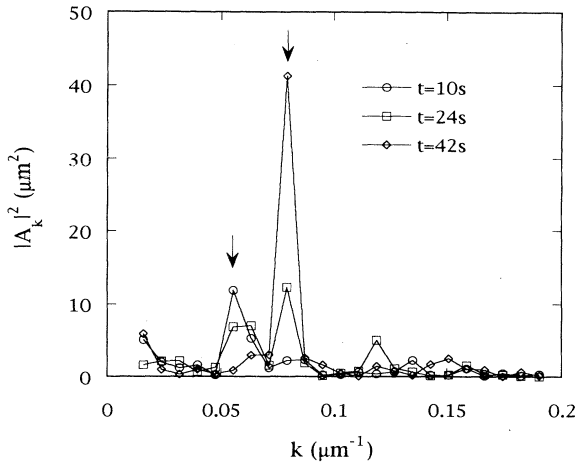

FIG. 8. Spectra of the sequence of images displayed in Fig. 7. The initial wave vector is shown by the left arrow. The final one is shown by the right arrow and corresponds to the morphology after the new-birthed cell.

For this purpose, we expand $\Omega(k^2,\varepsilon)$ as

$$\Omega(k^2,\varepsilon)\cong a\varepsilon-b(k^2-k_c^2)^2 , \tag{20}$$

where $a\equiv\partial\Omega/\partial\varepsilon$ and $b\equiv-0.5\partial^2\Omega/\partial(k^2)^2$ with both derivatives calculated at the bifurcation. Using also the approximation $k^2-k_c^2\cong 2k_cq$, with $q\equiv k-k_c$, we obtain, by substituting Eq. (20) into Eq. (19), the phase diffusion coefficient valid near the bifurcation:

$$D\approx 4k_c^2b\left[\frac{q_m^2-3q^2}{q_m^2-q^2}+\frac{q}{k_c}\right] , \tag{21}$$

where $q_m^2\equiv a\varepsilon/(4bk_c^2)$. The first term inside the brackets of the above equation is even in q and reproduces the classical result [25]. The novelty is the term q/k_c, which is responsible for the tilting of the Eckhaus boundary.

Equation (21) shows why the tilting is so effective, even very near the bifurcation, as first observed by Misbah and co-workers in their numerical results.

B. Experimental results

In this section we present experimental results on the measurements of the spatial wave vector of the nematic-isotropic interface. For pulling velocities above the critical one we observed, in some circumstances, a nonconstant wave vector during the time evolution of the unstable interface. This migration of the wave vector was always towards greater values and more noticeable for small gradients. An example of this effect can be seen in the time sequence of interface shapes shown in Fig. 7, and in their power spectra displayed in Fig. 8. It is possible to think about this phenomenon as being caused by an Eckhaus instability, which is a hypothesis that we want to test. We present here the results of our wave-vector measurements, during the cellular instability, and compare them with the calculations developed in the preceding section.

In the first qualitative observation of an Eckhaus instability in directional solidification done by Simon, Bechhoefer, and Libchaber [29], they observed phase instabilities on a stationary pattern, after abruptly changing the pulling velocity. Differently, in our experiments we observe the transient dynamics at constant velocity and temperature gradient. The wave-vector migration that we observed is not associated with an abrupt change between two different states of the pattern. In Figs. 9(a) and 9(b) we present the final wave vectors measured in our experiments, represented by the triangles, for the temperature gradients of 43.3 K/cm and 25 K/cm, for different pulling velocities, and their location inside the linear unstable region. The Eckhaus band was calculated using Eq. (19) of the preceding section.

In all cases, the initial and final wave vectors were located inside the lower wave-vector side of the unstable Eckhaus band. One notices that the observed final wave vectors do not exactly match the Eckhaus boundary. These results suggest that other mechanisms of pattern selection might be operating.

In a recent article, Warren and Langer [33] proposed a different mechanism for pattern selection in directional solidification. They argue that the cellular instability may occur while the impurity concentration field is still in a nonsteady state. By considering a nonsteady concentration profile, they predict a wave-vector migration, from lower to higher values, since the front velocity is changing with time (from a lower to a higher value) and so the corresponding Mullins-Sekerka dispersion curve. In this interpretation there is not actually a phase instability, but a change of the maximum-growth-rate wave vector, following the changes in the concentration field. This model displays a strong selection of a particular wave vector. A detailed test of this model is under way in our laboratory, and will be the subject of a future publication.

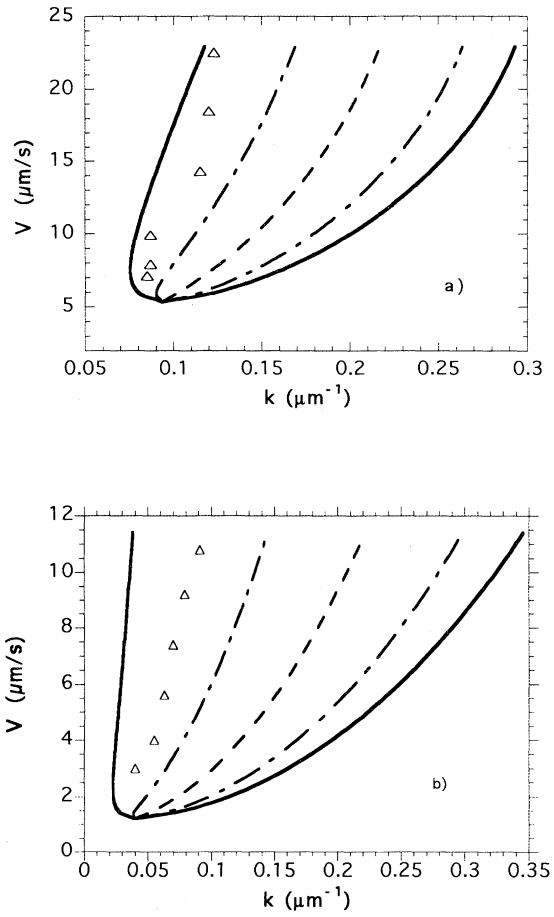

FIG. 9. Experimental values for the final wave vector and its location inside the linear unstable region. Curves were calculated using the parameters of Table III, with kinetics. (a) Data for $G=43.3$ K/cm. (b) Data for $G=25$ K/cm. Note that the experimental wave vectors are inside the unstable Eckhaus region.

V. CONCLUSIONS

In this paper we have presented a detailed account of our experiments on the planar-cellular instability of a moving nematic-isotropic interface of the liquid crystal 8CB and a brief review of the two-sided model of solidification. In order to compare our results with the two-sided model we looked for a parameter region where the planar-cellular instability could adequately be described by a third-order Landau-amplitude equation. This was possible because the planar-cellular bifurcation for the nematic-isotropic interface is supercritical, such that, near the bifurcation, very few modes are unstable. The instability growth rates as well as the obtained cubic coefficients are in agreement with the two-sided model. When kinetic effects are included, an alternative expression for the growth rate of the instability is obtained. The experimental data are still very well fitted by this expression, with parameters that are close to the ones obtained without kinetic effects. The values for the parameters that resulted from the fittings are reasonable for liquid crystals, with the exception of the capillary length, whose value was of the order of 100 times larger than the one predicted by the Gibbs-Thomson relation. The addition of elastic contributions from the nematic phase to the interface free energy, as considered by Bechhoeffer and Langer, and the coupling between impurity diffusion and the nematic director field by Misbah and Valance, were not enough to solve this discrepancy. Therefore, it is still lacking a complete understanding of the stabilizing mechanism for the moving nematic-isotropic interface during a directional solidification experiment.

Since the linear analysis predicts a continuous band of wave vectors, we attempted to explain the final values for the wave vectors observed in our experiments, based on an Eckhaus instability. In order to do that, we first performed an analytical calculation of the Eckhaus boundary for solidification. The interesting result is that, even for a calculation based on an amplitude equation, we were able to obtain a tilted Eckhaus boundary, a feature that was previously believed to show up only in numerical work of complete models of solidification, such as the symmetric model. It was believed that to explain this feature, the interaction between a great number of modes would be necessary. Since an amplitude-equation approach is a simplification of the dynamics where very few modes are active, we conclude that the tilting of the Eckhaus boundary is not due to the presence of many modes interacting, but due to the properties of the dispersion curve of the linear problem. We have obtained a general expression for the phase diffusion coefficient of the pattern. It allowed us to calculate the Eckhaus boundary for the two-sided model, by using the parameters obtained previously from the linear analysis. Our results for the final wave vectors do not support the hypothesis of an Eckhaus instability as a pattern-selection mechanism in our experiments. Therefore, other mechanisms must be searched. In particular, the mechanism proposed by Warren and Langer, where a nonsteady concentration profile is considered, seems promising. Investigations for checking this proposal are under way in our laboratory.

ACKNOWLEDGMENTS

This work was supported by the Brazilian Agencies Conselho Nacional de Desenvolvimento Cientifico e Tecnológico (CNPq) and Fundação de Amparo à Pesquisa do Estado de Minas Gerais (FAPEMIG).

[1] M. C. Cross and P. C. Hohenberg, Rev. Mod. Phys. **65**, 851 (1993).
[2] W. W. Mullins and R. F. Sekerka, J. Appl. Phys. **34**, 232 (1963); **35**, 444 (1964).
[3] D. J. Wollkind and L. A. Segel, Phyl. Trans. R. Soc. **268**, 351 (1970).
[4] S. de Cheveigné, C. Guthmann, P. Kurowski, E. Vicente, and H. Biloni, J. Cryst. Growth **92**, 616 (1988).
[5] B. Caroli, C. Caroli, and B. Roulet, J. Phys. (Paris) **43**, 1767 (1982).
[6] P. Oswald, J. Bechhoefer, and A. Libchaber, Phys. Rev. Lett. **58**, 22 (1987).
[7] A. J. Simon and A. Libchaber, Phys. Rev. A **40**, 7090 (1990).
[8] P. Coullet and G. Iooss, Phys. Rev. Lett. **64**, 866 (1990).
[9] J. M. Flesselles, A. J. Simon, and A. Libchaber, Adv. Phys. **40**, 1 (1991).
[10] J. T. C. Lee and R. A. Brown, Phys. Rev. E **47**, 4937 (1993).
[11] J. S. Langer, Rev. Mod. Phys. **52**, 1 (1980).
[12] H. Chou and H. Z. Cummins, Phys. Rev. Lett. **61**, 173 (1988).
[13] J. M. A. Figueiredo, M. B. L. Santos, L. O. Ladeira, and O. N. Mesquita, Phys. Rev. Lett. **71**, 4397 (1993).
[14] J. Bechhoefer and S. A. Langer, Phys. Rev. E **51**, 2356 (1995).
[15] J. D. Hunt, K. A. Jackson, and H. Brown, Rev. Sci. Instrum. **37**, 805 (1966).
[16] BDH Chemicals Ltd., Poole BH12 4NN, Eng., BHD Liquid Crystals Catalog.
[17] Merck Extran 7553.
[18] Merck ZLI 3334.
[19] J. Bechhoefer, A. J. Simon, and A. Libchaber, Phys. Rev. A **40**, 2042 (1989).
[20] S. R. Coriell and R. F. Sekerka, J. Cryst. Growth **61**, 499 (1983).
[21] L. D. Landau and E. M. Lifshitz, *Física Estadística* (Editorial Reverté, Barcelona, 1975).
[22] H. Marynissen, J. Thonen, and W. Van Kael, Mol. Cryst. Liq. Cryst. **97**, 149 (1983).
[23] S. Ghodbane and D. E. Martire, J. Phys. Chem. **91**, 6410 (1987).
[24] C. Misbah and A. Valance, Phys. Rev. E **51**, 1282 (1995).
[25] B. Caroli, C. Caroli, and B. Roulet, *Instabilities of Planar Solidification Fronts,* in *Lecture Notes of L'Ecole de Physique de Matière Condensée* (Beg-Rohu, France, 1989).
[26] Paul Manneville, *Dissipative Structures and Weak Turbulence* (Academic, San Diego, 1990).
[27] W. Eckhaus, *Studies in Nonlinear Stability Theory* (Springer, New York, 1965).
[28] M. Lowe, J. P. Gollub, and T. C. Lubensky, Phys. Rev. Lett. **51**, 786 (1983); M. Lowe and J. P. Gollub, *ibid.* **55**, 2575 (1985).
[29] A. J. Simon, J. Bechhoefer, and A. Libchaber, Phys. Rev. Lett. **61**, 2574 (1988).
[30] E. Hernández-Garcia, J. Viñals, R. Toral, and M. San Miguel, Phys. Rev. Lett. **70**, 3576 (1993).
[31] A. Ghazali and C. Misbah, Phys. Rev. A **46**, 5026 (1992).
[32] K. Brattkus and C. Misbah, Phys. Rev. Lett. **64**, 1935 (1990).
[33] James A. Warren and J. S. Langer, Phys. Rev. E **47**, 2702 (1993).

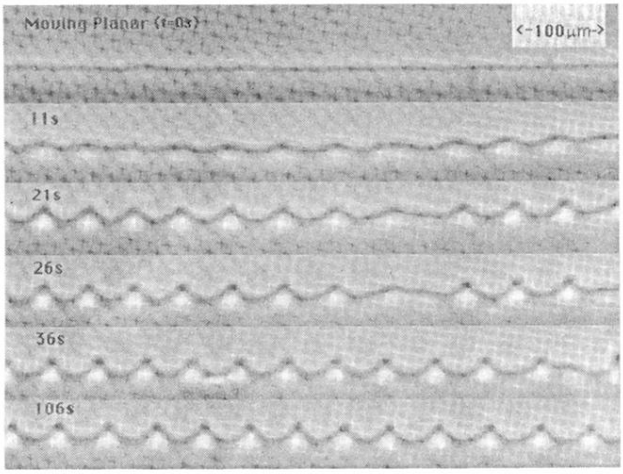

FIG. 2. Sequence of images showing the interface at different times. The nematic phase is above and the isotropic one is below the interface. Experiment performed with $G = 43.3$ K/cm and $V = 18.5\ \mu$m/s.

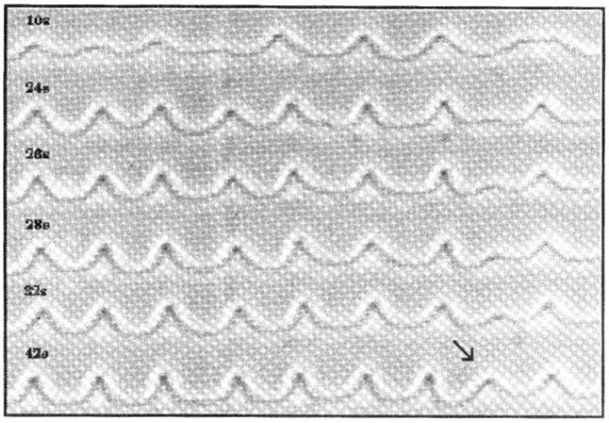

FIG. 7. Sequence of images showing the birth of a new cell during the time evolution of the interface's morphology. Experiment performed at $G = 25$ K/cm and $V = 5.7$ μm/s.